drones

MDPI

Article

Backhaul-Aware User Association and Throughput Maximization in UAV-Aided Hybrid FSO/RF Network

Muhammad Nafees *, Shenjie Huang, John Thompson and Majid Safari

School of Engineering, Institute for Digital Communications, The University of Edinburgh, Edinburgh EH9 3JL, UK
* Correspondence: m.nafees@ed.ac.uk

Abstract: Free-space optical (FSO) communication is expected to play an indispensable role with high data rates and low system complexity in beyond fifth-generation (B5G) networks. However, infrequent adverse weather conditions can incapacitate its performance. The combination of FSO and radio frequency (RF) has emerged as an effective alternative for meeting the growing need for high data rates in wireless communication networks. Unmanned aerial vehicles (UAVs) are also anticipated to play an instrumental role in B5G networks due to their flexible movement and deployment. In this paper, a UAV-aided hybrid FSO/RF backhauling system using a matching game theory (GT) and reinforcement learning (RL) framework is investigated. We deploy a UAV to provide a user offloading service to an already existing ground base station (GBS), which is facing a reduced backhaul capacity due to weather attenuation (e.g., fog). It is considered that the GBS has a pre-installed FSO backhaul connection to a macro-base station (MBS). However, during adverse weather conditions, the FSO backhaul is severely affected, compromising the reliability of the FSO link. With the reduced FSO backhaul capacity, the GBS needs an additional backhaul link to support its backhaul data transmission to the destination MBS. As a result, instead of building an expensive permanent parallel RF link for the rare foggy situation, a UAV can be hired to serve a portion of the users, thereby reducing the GBS load. The users perform a matching game-based procedure to select the base station (BS) of their choice to maximize their utility. The UAV is deployed at an optimal altitude, and the bandwidth partition between the GBS and the UAV is optimized to maximize the system throughput using RL. Real weather data from the cities of Edinburgh and London in the U.K. are used to evaluate the performance of the system. The numerical results show the superiority and effectiveness of the proposed scheme compared to conventional methods.

Keywords: free space optics (FSO); matching game theory (GT); reinforcement learning (RL); unmanned aerial vehicle (UAV)

Citation: Nafees, M.; Huang, S.; Thompson, J.; Safari, M. Backhaul-Aware User Association and Throughput Maximization in UAV-Aided Hybrid FSO/RF Network. *Drones* **2023**, *7*, 74. https://doi.org/10.3390/drones7020074

Academic Editors: Iván Vidal and Francisco Valera

Received: 16 December 2022
Revised: 13 January 2023
Accepted: 16 January 2023
Published: 19 January 2023

1. Introduction

Data rates on the order of terabits per second are expected as wireless technology evolves beyond fifth-generation (B5G) networks. To properly evaluate the B5G wireless networks, new technical requirements, dynamic communication scenarios, and performance indicators are introduced [1]. Unmanned aerial vehicles (UAVs) have been widely proposed to support existing networks in providing wireless communication services anywhere and at any time to enable flexible movement, powerful computing, etc. [2]. In addition to the rising demand for UAVs, relay stations and small cells are expected to be widely deployed to improve mobile data coverage, necessitating high-speed backhauling. To address these issues, free-space optical (FSO) communication has been identified as a promising wireless technology for high-capacity, cost-effective, and energy-efficient communication networks with data rates comparable to optical fiber links [3,4]. The FSO link's wireless functionality offers a suitable communication system for both dense urban and rural locations as well as

areas prone to fiber cut failures. In fact, FSO systems are expected to be critical in emerging network architectures such as cell-free technology [5].

However, practical FSO systems face some limitations and challenges, such as pointing and misalignment loss due to building sways, turbulence-induced intensity fluctuation (also known as scintillation), and adverse weather conditions such as fog and snow [6,7]. In particular, FSO links can be severely hampered by a fog event, which is a relatively long-lasting yet infrequent phenomenon. In contrast, fog has practically a nominal impact on radio frequency (RF) systems; therefore, one possible solution is to build hybrid FSO/RF links [8]. However, given the increasing demand for FSO links and the massive expansion of cell sites, it is reasonable to assume that not all FSO links can have parallel RF transmission links for various reasons such as the high link expense. Moreover, adverse weather conditions such as fog are not frequent in many geographical areas. For example, official weather data from the Meteorological Office of the United Kingdom show that the city of Edinburgh experienced only 86 h of fog events (visibility < 1 km) from January 2016 to June 2017, which is only almost 0.65% of the specified duration [6]. To this end, temporary solutions can be envisaged rather than permanent, expensive RF links.

Motivated by the growing demand for UAV deployment as relays, we propose a UAV-aided user offloading scheme using matching game theory (GT) and reinforcement learning (RL), in particular Q-learning. This approach can enhance the throughput of a ground base station (GBS) to the macro-base station (MBS) supported by a fog-troubled FSO backhaul link. The UAV can establish a temporary RF backhaul link (e.g., millimeter wave) with the MBS in adverse weather conditions. The UAV relay offloads users from the coverage area of the GBS. The FSO channel condition determines the optimal placement of the UAV, which defines the coverage ratio of the GBS and UAV to maximize the end-to-end network throughput. As the adverse weather event passes, the UAV may be withdrawn and the GBS can resume regular operation without a UAV relay. We refer to our proposed scheme as **c**apacity-aware **U**AV deployment and **re**source allocation (CURE) and its suboptimal version as **c**ell-edge-based **U**AV **de**ployment (CUDE). We also compare the performance of the proposed scheme with the state-of-the-art schemes, which include GBS-only (GBSO), e.g., traditional FSO backhauling without UAV, and **C**ell **a**ssociation with **r**ange **e**xpansion (CARE).

Related Work and Contribution

The emergence of UAV technologies has created new potential for a wide range of applications [9]. Under many network scenarios, UAVs are becoming more popular for user offloading. For instance, the authors of [10] evaluated the impact of UAV altitude and transmit power, as well as the offload portion, on the user's downlink sum rate, assuming that UAV to user links are line-of-sight (LoS) channels. To provide downlink data offloading in some areas of a BS, the work in [11] temporarily deployed UAVs. The method utilizes contract theory to model the situation, where the BS manager must develop an optimal contract to maximize its own revenue. By jointly optimizing the UAV's trajectory, bandwidth allocation, and user partitioning, Lyu et al. [12] proposed an aerial mobile BS to offload data traffic for cell-edge users. In [13], the heterogeneous UAV-enabled data offloading is modeled in an innovative framework to dynamically estimate user status information and determine the UAV scheduling strategy, whose purpose is to lower the user data queue length while extending the working time of the UAV.

Machine learning (ML)-based optimization solutions are increasingly considered in the context of UAV-assisted networks. For instance, reference [14] discussed various ML methods for developing UAV-assisted radio access networks, with a special emphasis on supervised ML and RL procedures with high-speed backhaul links (e.g., FSO). Fan et al. [15] investigated the UAV-enabled traffic offloading problem under a mixed user traffic scenario, where delay-sensitive user traffic and delay-insensitive user traffic are jointly considered, and a deep neural network-powered genetic algorithm is used to obtain the optimal association between the UAVs and the ground systems. The authors

of [16] used a multiarmed bandit-based offload path selection scheme to address the issue of decentralized data offloading in an edge UAV swarm. This is to reduce the complexities of a single UAV repeatedly producing and processing large amounts of application-specific data. In UAV networks, a combination of ML and GT is also regarded as a promising technique. For example, Gao et al. [17] proposed a game-based multi-agent deep deterministic policy gradient approach for optimizing the trajectory of multiple UAVs while taking into account users' offloading delay, energy efficiency, and the use of an obstacle avoidance system. The work in [18] adopted a novel game-theoretic and RL framework for computational offloading in a multi-service provider mobile edge computing network. Li et al. [19] investigated a joint optimization of beamforming and beam-steering in multi-UAV millimeter wave networks considering LoS communication for UAVs, where beamforming and beam-steering optimizations were carried out using an ML-inspired algorithm and a mean field GT scheme, respectively.

Several studies have considered UAVs for offloading, capacity enhancement, and relaying services. However, only a few studies have addressed both UAV-assisted networks and FSO backhauling to provide network service. The study in [20] investigated the 3D deployment and resource allocation of a UAV in a hotspot area to maximize access link throughput given constraints on user quality-of-service (QoS), FSO backhaul link capacity, and total bandwidth and power. However, the backhaul constraint is eased by assuming an ideal, high-capacity FSO backhaul. To maximize the network throughput, the authors of [21] considered the association between aerial and terrestrial terminals, transmit power, and the deployment of multiple UAVs, wherein backhaul-to-relay and relay-to-user communications employed FSO and RF links, respectively. In [22], a hovering UAV-based serial FSO decode-and-forward relaying system that considers various types of channel impairments is investigated to improve system performance by optimizing the beam width, field of view, and UAVs' locations. Ajam et al. [23] proposed a UAV-aided communication system with RF access links to mobile users and an FSO backhaul link to analyze the end-to-end system performance of a network in terms of the ergodic sum rate by optimizing the placement of UAV that serve as buffer-aided and non-buffer-aided relays. By jointly designing the FSO and RF links and the UAV altitude, the study in [24] maximized the system-level energy efficiency, which is equivalently expressed as the ratio of the UAV's multicasting rate over the optics BS transmit power, subject to the UAV's sustainable operation and reliable backhauling constraints. The work in [25] investigated the 3D location of the drone BS, user association, and bandwidth allocation policy between the MBS and the drone BS in order to minimize the total average latency ratio of all users while maintaining each user's QoS requirement. However, these studies have not taken into account the weather's impact on FSO backhaul, which is crucial in the FSO link availability and consequently impacts the UAV deployment.

This work can be considered as one of the pioneering studies toward hybrid FSO/RF networks under the umbrella of B5G networks, which are envisioned to integrate a combination of FSO, UAVs, and high-speed RF (e.g., millimeter wave) technology for diverse scenarios. The main contributions of this study are stated below.

Contributions: The main contributions of this study are stated below.

- We investigate a scenario where a UAV provides user offloading service to a GBS, which has an FSO backhaul connection to the MBS. Specifically, the objective is to maximize the network's overall end-to-end throughput with the aid of a UAV when the GBS's FSO backhaul link is not reliable due to adverse weather conditions. We propose an FSO backhaul-aware matching GT and RL-based solution for optimal user association and overall network throughput maximization. The users decide for themselves which BS (GBS or UAV) they would like to be associated with to increase their utility (data rate).
- The paper proposes a two-layer system, where a matching GT technique is employed at the lower layer to associate users with the GBS or UAV that maximizes their utility. The system is then trained using RL to optimize the UAV's altitude and

bandwidth partitioning based on the weather conditions. The proposed scheme does not require users to be aware of other players' actions, which can greatly reduce the communications overhead. In addition, once the training is completed, the system can quickly obtain optimal parameters (altitude and bandwidth partition) for any random user distribution.

- Lastly, the proposed hybrid network framework is evaluated under different weather conditions including realistic weather statistics from the cities of Edinburgh and London in the UK. The results clearly indicate the supremacy of the proposed approach over GBS-only and two other benchmark user association schemes.

We organize the rest of this article as follows. The system model of the proposed UAV-aided hybrid FSO/RF network is presented in Section 2. The problem formulation and resource allocation using a matching GT and RL framework are detailed in Section 3. The complexity and convergence analysis of the proposed scheme are also given in Section 3. Some numerical results are presented in Section 4, and results based on practical weather measurements are also discussed in Section 4. Finally, the paper is concluded in Section 5.

2. System Model

The schematic of the proposed system for high-speed wireless backhauling of a GBS is shown in Figure 1. We assume that a preinstalled FSO link exists between the GBS and the MBS. In the context of B5G, the GBS could be in the same coverage area as MBS, e.g., heterogeneous network or in a remote location, e.g., relay station. FSO-based wireless backhauling solutions are very reliable and offer high achievable data rates in more frequent normal weather conditions. So, in addition to the existing FSO link, installing a parallel high-speed RF link between GBS and MBS just for occasional use in adverse weather events is redundant, expensive (e.g., RF licensing costs), and difficult to maintain considering the large number of anticipated BSs in B5G. When the FSO backhaul capacity drops below a minimal threshold C_{th} because of the adverse weather conditions, e.g., fog events, the GBS would like to maximize the utilization of its licensed sub-6 GHz spectrum W in the downlink. It takes advantage of the UAV's services to help some users by letting the UAV use some portion of W, which should be efficiently shared between the two BSs. In addition, the UAV can establish a temporary LoS link for backhaul with any nearby node, including the MBS. Owing to its higher capacity and active beam steering, millimeter wave backhauling outperforms sub-6 GHz backhauling across the RF spectrum [26]. Hence, it is assumed that the UAV establishes a backhaul link to the MBS using an ideal high-speed directional millimeter wave link.

Due to the increased density of BS nodes in B5G, it is impractical to equip every GBS node with an expensive and difficult-to-maintain parallel high-speed RF backhaul. As a result, it is anticipated that a UAV is equipped with a high-performance millimeter-wave transceiver designed to operate in the scenarios such as depicted in Figure 1. Millimeter-wave communications using the large bandwidth over 28 GHz is promising for high-rate UAV transmissions [27]. It is also worth pointing out that instead of the MBS, the UAV can also establish a backhaul connection with any nearby RF node, which might not have an LoS connection possibility with the GBS. Note that this assumption is justified because the foggy conditions have a negligible impact on RF signals. Hence, the system could now be referred to as a hybrid FSO/RF backhauling system, since both FSO and RF technologies are used at the backhaul links, i.e., FSO backhaul for the GBS and millimeter wave backhaul for the UAV. As the fog event passes, the UAV may be withdrawn because the FSO backhaul link of the GBS can resume regular operation. Furthermore, we assume that in the downlink, both BSs use omnidirectional antennas. Next, a brief description of the channel models is provided.

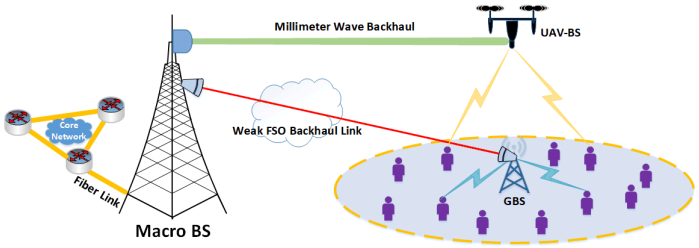

Figure 1. The proposed system model for UAV-aided user offloading in adverse weather conditions.

2.1. FSO Channel Model

Given that the FSO link employs intensity modulation direct detection (IM/DD), the received electrical signal expression can be written as

$$s_{\mathrm{o}} = \rho g_{\mathrm{o}} h_{\mathrm{o}} x_{\mathrm{o}} + z_{\mathrm{o}}, \tag{1}$$

where ρ is the responsivity of the photodetector, g_{o} refers to the average channel gain, h_{o} denotes the random turbulence-induced intensity fading, x_{o} is the transmitted optical intensity, s_{o} is the received electrical signal and z_{o} is zero-mean real Gaussian noise with variance σ_{o}^2. Note that we use the subscript 'o' to denote the optical link. The signal-independent Gaussian noise z_{o} in (1) arises from thermal noise as well as the shot noise induced by the ambient light. The average gain g_{o} could be expressed as [6,28]

$$g_{\mathrm{o}} = \left[\mathrm{erf}\left(\frac{\sqrt{\pi} d}{2\sqrt{2}\phi L_{\mathcal{SD}}} \right) \right]^2 \times \exp\left(-\vartheta L_{\mathcal{SD}}\right), \tag{2}$$

where the first and second terms are the geometric loss due to the divergence of the transmitted beam and the atmospheric loss due to scattering and absorption, respectively. The receiver aperture diameter is denoted by d, ϕ is the beam divergence angle, $L_{\mathcal{SD}}$ is the distance between the source and the destination, and ϑ is a weather-dependent attenuation coefficient determined based on the Beer–Lambert law. The relationship between ϑ and the visibility V in km can be expressed as $\vartheta = \frac{3.91}{V}\left(\frac{\lambda_{\mathrm{o}}}{550 \times 10^{-9}}\right)^{-\xi}$ [29], where ξ is the weather condition-based size distribution of the scattering particles. It can be expressed as a function of the visibility distance as [30]

$$\xi = \begin{cases} 1.6, & V > 50\,\mathrm{km} \\ 1.3, & 6\,\mathrm{km} < V < 50\,\mathrm{km} \\ 0.16V + 0.34, & 1\,\mathrm{km} < V < 6\,\mathrm{km} \\ V - 0.5, & 0.5\,\mathrm{km} < V < 1\,\mathrm{km} \\ 0, & V < 0.5\,\mathrm{km}. \end{cases} \tag{3}$$

The log-normal distribution and the Gamma–Gamma distribution are two common methods for modeling the turbulence-induced intensity fluctuation h_o. We use the Gamma–Gamma distribution, which can characterize the intensity function under a variety of turbulence situations as [6,31]

$$f_{\mathrm{o}}(h_{\mathrm{o}}) = \frac{2(\bar{\alpha}\bar{\beta})^{(\bar{\alpha}+\bar{\beta})/2}}{\Gamma(\bar{\alpha})\Gamma(\bar{\beta})} h_{\mathrm{o}}^{(\bar{\alpha}+\bar{\beta})/2-1} K_{\bar{\alpha}-\bar{\beta}}\left(2\sqrt{\bar{\alpha}\bar{\beta}h_{\mathrm{o}}}\right), \tag{4}$$

where $\Gamma(.)$ denotes the Gamma function, and $K_p(.)$ is the modified Bessel function of the second type. The parameters $\bar{\alpha}$ and $\bar{\beta}$ are defined as [32]

$$\bar{\alpha} = \left[\exp\left(\frac{0.49\mho^2}{\left(1 + 0.18\varkappa^2 + 0.56\mho^{12/5}\right)^{7/6}} \right) - 1 \right]^{-1},$$
$$\bar{\beta} = \left[\exp\left(\frac{0.51\mho^2 \left(1 + 0.69\mho^{12/5}\right)^{-5/6}}{\left(1 + 0.9\varkappa^2 + 0.62\varkappa^2\mho^{12/5}\right)^{5/6}} \right) - 1 \right]^{-1},$$

where $\mho^2 = 0.5C_n^2 k^{7/6} L_{\mathcal{SD}}^{11/6}$, $\varkappa^2 = kd^2/4L_{\mathcal{SD}}$ and $k = 2\pi/\lambda_o$. Note that C_n^2 is the turbulence refraction structure parameter. The achievable rate (channel capacity lower bound) conditioned on the random channel gain h_o for the IM/DD FSO channel described in (1) can be stated as [6,33]

$$C_o = \frac{W_o}{2} \log_2 \left(1 + \frac{e\rho^2 g_o^2 h_o^2 \zeta_o^2}{2\pi\sigma_o^2} \right), \tag{5}$$

where W_o is the optical bandwidth, e is the base of natural logarithm and ζ_o represents the optical transmission power of the FSO node (e.g., MBS).

Strong atmospheric turbulence is highly unlikely during a fog event due to their inverse correlation [34], but it cannot be totally ignored. It is worth noting that due to a very small coherence time (i.e., rapid changes), UAV deployment and resource allocation are unable to respond to channel capacity fluctuations caused by scintillation. To cope with this problem and to encounter the impact of turbulence on the proposed system, we use a sliding window averaging strategy [6,35] to smooth out the rapid FSO link capacity fluctuations. Note that a window with a longer interval than the scintillation coherence time (which is on the order of milliseconds) should be used so that the average FSO link capacity can accurately reflect long-term weather conditions. The average FSO link capacity is measured over the window interval, which is estimated as $\bar{C}_o = E[C_o]$, where $E[.]$ denotes the ensemble expectation. The GBS can monitor the condition of the FSO link and calculate $\bar{C}_o$ every window interval. When $\bar{C}_o$ falls below a certain threshold, C_{th}, the services of a UAV may be required to offload some users—in the worst case, all users due to the total non-functionality of the FSO link. To ensure that the GBS can respond quickly to changing weather conditions, the window interval should be significantly shorter than the time-scale of the weather changes, which is on the order of hours.

2.2. RF Channel Model

2.2.1. Air to Ground Channel

The wireless air-to-ground (AtG) channel between a UAV and a ground user is primarily composed of two components: the LoS component and the non-LoS (NLoS) component. The probability of establishing an LoS link between a user and the UAV with an elevation angle of θ (in degrees) is given by [10]

$$P_L^{ak}(\theta) = \frac{1}{1 + \omega_1 \exp\left(-\omega_2[\theta - \omega_1] \right)}, \tag{6}$$

where ω_1 and ω_2 are constant parameters which depend on the carrier frequency and the communication environment. In addition, $\theta = \frac{180}{\pi} \times \sin^{-1}\left(\frac{\mathcal{H}}{d_{ak}}\right)$ is the elevation angle between the kth user and the UAV with $d_{ak} = \sqrt{(x_k - x_a)^2 + (y_k - y_a)^2 + \mathcal{H}^2}$, the total distance between kth user and the UAV, which has an altitude $\mathcal{H}$. Then, the average path loss (PL) $\overline{\mathcal{L}}_{ak}$ can be expressed as [36,37]

$$\begin{cases} \overline{\mathcal{L}}_{ak} = P_L^{ak}(\theta) \cdot \mathcal{L}_{ak}^{\mathrm{LOS}} \\ \qquad\qquad + \left[1 - P_L^{ak}(\theta)\right] \cdot \mathcal{L}_{ak}^{\mathrm{NLOS}}, \\ \mathcal{L}_{ak}^{\mathrm{LOS}} = \Gamma_1 \left(\dfrac{4\pi f_c d_{ak}}{c}\right)^{\eta}, \\ \mathcal{L}_{ak}^{\mathrm{NLOS}} = \Gamma_2 \left(\dfrac{4\pi f_c d_{ak}}{c}\right)^{\eta}, \end{cases} \tag{7}$$

where f_c is the carrier frequency, c denotes the speed of light and η is the PL exponent. The PL values of the LoS and NLoS components are represented by $\mathcal{L}_{ak}^{\mathrm{LOS}}$ and $\mathcal{L}_{ak}^{\mathrm{NLOS}}$, respectively. In addition, Γ_1 and Γ_2 denote the additional PL, which depends on the type of communication environment.

2.2.2. Ground-to-Ground Channel

The GBS-to-user channels are only considered NLoS because the elevation angle between them is small. In effect, there is a high probability of NLoS links, which defines the PL as [11]

$$\overline{\mathcal{L}}_{sk} = \Gamma_2 \left(\frac{4\pi f_c d_{sk}}{c}\right)^{\eta}, \tag{8}$$

where $d_{sk} = \sqrt{(x_k - x_s)^2 + (y_k - y_s)^2 + \mathcal{H}_s^2}$ is the GBS to user distance, and $\mathcal{H}_s$ denotes the altitude of the GBS.

2.3. Cell-Edge-Based UAV Altitude

In a traditional UAV deployment technique [38–41], the edge user (cell-edge) is considered while positioning the UAV to enhance the QoS of the farthest users. At an optimal elevation angle θ_{edge}, the coverage radius is maximized for a predefined PL value. Equivalently, there is an optimal altitude at which the PL at the cell-edge is minimized for a given radius. Let $\mathcal{H}_{edge}$ denote the optimal altitude that minimizes the PL at the cell-edge and r_s be the coverage radius of the area in Figure 1. Hence, by taking the partial derivative of (7), an equation of the critical point could be developed as [41]

$$\frac{\partial r_s}{\partial \mathcal{H}_{edge}} = \frac{\pi \mathcal{H}_{edge}}{9\ln(10)} + \frac{r_s \omega_1 \omega_2 \Gamma_d e^{\left(-\omega_2\left[\theta_{edge} - \omega_1\right]\right)}}{\left(\omega_1 e^{\left(-\omega_2\left[\theta_{edge} - \omega_1\right]\right)} + 1\right)^2} = 0, \tag{9}$$

where $\Gamma_d = (\Gamma_1 - \Gamma_2)$ and $\theta_{edge} = \frac{180}{\pi} \arctan(\frac{\mathcal{H}_{edge}}{r_s})$ is the elevation angle of an edge user. Therefore, cell-edge-based optimal UAV altitude $\mathcal{H}_{edge}$ can be obtained from (9), which is widely adopted to determine the optimal altitude in UAV networks. It is worth noting that the UAV altitude obtained from (9) serves as a benchmark for the proposed model and a backhaul-aware UAV altitude optimization is performed in Section 3.2.

2.4. User Distribution and Cell Association

We assume that K users are uniformly and independently distributed in the coverage area using a homogeneous Poisson point process, which is obtained through a spatial point process. Let $\mathcal{K} = \{1, 2, ..., K\}$ denote the set of users and $\mathcal{M} = \{a, s\}$ be the set of two BSs (UAV and GBS). We employ a widely used cell association strategy known as reference signal received power (RSRP) [42] for the initial user association because of the flexibility it provides to users. The policy allows the kth user to be associated with the BS m that has the strongest RSRP ζ_{mk} as

$$m^* = \arg \max_{m \in \mathcal{M}}, \zeta_{mk}, \forall k \in \mathcal{K}, \forall m \in \mathcal{M}. \tag{10}$$

In addition, it is considered that the users can only be associated with one BS. To this end, a user association matrix $\hat{\mathcal{K}}$ can be developed as

$$x_{mk} = \begin{cases} 1, \text{if } k\text{th user associates with BS}_m, \\ 0, \text{ otherwise.} \end{cases} \tag{11}$$

It is important to note that for the proposed model, an initial user association policy is given in (10) and a backhaul-aware optimal policy is devised in Section 3.1.

3. Problem Formulation and Resource Allocation

In this paper, we assume that bandwidth W is shared between the two BSs based on a bandwidth allocation factor Ψ that can be adjusted to efficiently manage the bandwidth partition. Hence, $W_\mathrm{a} = \Psi W$ is the bandwidth used by the UAV and $W_\mathrm{s} = (1-\Psi)W$ is allocated to the GBS. Consider that both GBS and UAV broadcast at fixed transmit powers of $\zeta_\mathrm{T}^\mathrm{s}$ and $\zeta_\mathrm{T}^\mathrm{a}$, respectively. Thus, the data rate achieved by the kth user associated with the GBS can be calculated as

$$\hat{\mathcal{R}}_k^\mathrm{s} = \frac{W_\mathrm{s}}{K_\mathrm{s}} \log_2\left(1 + \frac{\zeta_\mathrm{T}^\mathrm{s}/\overline{\mathcal{L}}_{\mathrm{s}k}}{N_\mathrm{p}}\right), \tag{12}$$

where K_s is the user-load for the GBS and N_p denotes the power of additive white Gaussian noise (AWGN). However, an unreliable backhaul can limit the user data rate and also incur delay. The rate constraint directly impacts the network throughput, whereas the delay constraint is critical for control signalling deadlines [43]. In this paper, we only consider the backhaul rate limitation which is caused by the weather attenuation. As a result, when the total access link throughput exceeds the FSO backhaul capacity, the user rate in (12) cannot be guaranteed. To this end, the effective throughput of the kth user could be expressed as

$$\mathcal{R}_k^\mathrm{s} = \begin{cases} \hat{\mathcal{R}}_k^\mathrm{s} & \text{if } \sum_{k=1}^{K_\mathrm{s}} \hat{\mathcal{R}}_k^\mathrm{s} \le \bar{C}_o \\ \dfrac{\hat{\mathcal{R}}_k^\mathrm{s} \bar{C}_o}{\sum_{k=1}^{K_\mathrm{s}} \hat{R}_k^\mathrm{s}} & \text{if } \sum_{k=1}^{K_\mathrm{s}} \hat{\mathcal{R}}_k^\mathrm{s} > \bar{C}_o. \end{cases} \tag{13}$$

Note that the fog-based attenuation is negligible for RF below 100 GHz frequencies [44]; hence it is assumed that the UAV can establish a reliable millimeter wave (e.g., 28 GHz) backhaul with capacity $\bar{C}_\mathrm{r}$ which is always sufficient to support the UAV's access link throughput, i.e., $\sum_{k=1}^{K_\mathrm{a}} R_k^\mathrm{a} \le \bar{C}_\mathrm{r}$. Then, the data rate of the kth user offloaded to the UAV could be calculated as follows

$$\mathcal{R}_k^\mathrm{a} = \frac{W_\mathrm{a}}{K_\mathrm{a}} \log_2\left(1 + \frac{\zeta_\mathrm{T}^\mathrm{a}/\overline{\mathcal{L}}_{\mathrm{a}k}}{N_\mathrm{p}}\right), \tag{14}$$

where K_a denotes the number of users offloaded to the UAV. Once the user association is completed, the sum throughput of UAV and GBS are, respectively, given as $\Phi_{UAV} = \sum_{k=1}^{K_\mathrm{a}} \mathcal{R}_k^\mathrm{a}$ and $\Phi_{GBS} = \sum_{k=1}^{K_\mathrm{s}} \mathcal{R}_k^\mathrm{s}$.

The proposed backhaul-aware system's goal is to maximize the total end-to-end throughput by optimizing the user's BS selection, the bandwidth partition Ψ between BSs, and the altitude $\mathcal{H}$ of the UAV. More formally, the following optimization problem P0 is formulated

$$\begin{aligned} (\mathrm{P0}): \quad & \max_{\hat{\mathcal{K}}, \Psi, \mathcal{H}} \quad \Phi_{GBS} + \Phi_{UAV} \\ & \text{s.t.} \quad x_{mk} = \{0,1\}, \forall m,k, && (15) \\ & \sum_{m=1}^{2} x_{mk} = 1, \forall k, && (16) \\ & 0 \le \Psi \le 1, && (17) \\ & \mathcal{H}_{min} \le \mathcal{H} \le \mathcal{H}_{max}, && (18) \end{aligned}$$

where constraints (15) and (16) ensure that each user must connect to only one BS. The constraints (17) and (18) represent the range of values for the bandwidth partition factor Ψ and UAV altitude $\mathcal{H}$, respectively. The value of $\mathcal{H}_{max}$ could be regarded as equivalent to $\mathcal{H}_{edge}$ in (9) because the UAV cannot provide better service above this altitude. Note that the association matrix $\hat{\mathcal{K}}$ can be influenced by UAV altitude and bandwidth partition, while the optimal value of Ψ would be different at different altitudes and vice versa. Hence, problem P0 is intractable owing to the interactions and coupled relationship between user association, UAV deployment, and bandwidth partition.

One efficient approach to solve P0 is to employ a hierarchical framework that combines GT and RL. The proposed framework decouples P0 into two-layer hierarchical sub-problems. Firstly, problem P1 (lower layer) presented in Section 3.1 deals with the backhaul-aware user association between the GBS and the UAV for a predefined Ψ and $\mathcal{H}$. This problem is solved by adopting a matching GT approach to provide an optimal user association in which users select the BS that offers a better utility (rate). Next, the second sub-problem P2 (upper layer) presented in Section 3.2 leverages RL to obtain the UAV altitude $\mathcal{H}$ and bandwidth partition Ψ that maximize the total system throughput according to the prevailing weather conditions. In essence, the objective of P2 is to acquire an optimal combination of bandwidth partition and UAV altitude denoted as Ψ_{opt} and $\mathcal{H}_{opt}$, respectively. P2 is iteratively solved by calling P1 for each combination of Ψ and $\mathcal{H}$ until the convergence is reached (total network throughput is maximized), which occurs at the optimum combination Ψ_{opt} and $\mathcal{H}_{opt}$. It is worth noting that the values of these optimal combinations could be different for different weather-dependent attenuation coefficients ϑ, hence making the RL process even more crucial, as will be shown and discussed in Section 4. Figure 2 depicts a visual representation of the hierarchical structure for solving P0 employing the matching GT and RL in Sections 3.1 and 3.2, respectively.

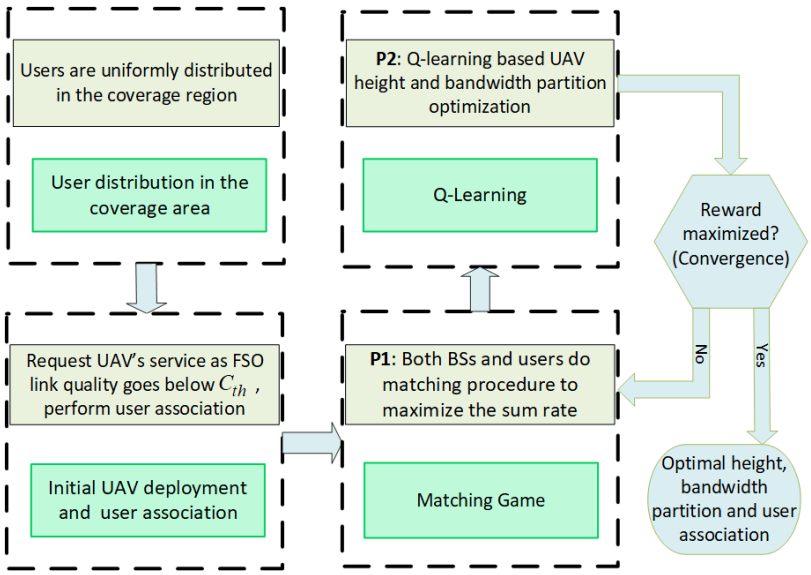

Figure 2. The framework for solving the problem of optimal user association, UAV deployment, and bandwidth partition.

3.1. Matching Game Formulation

The potential to model individual, independent decision makers with interactional strategies makes GT particularly appealing for analyzing wireless network performance. In contrast to conventional methods, GT can be used to construct robust and efficient distributed algorithms to address technical problems in UAV-assisted networks. Distributed solutions based on GT can help to reduce communication signal overhead [45]. In particular, the matching GT [46] can be used to provide solutions for combinatorial problems of

matching players in two disjoint sets to investigate how different types of rational and selfish players form dynamic and thus useful relationships.

It is worth noting that the proposed model completely matches a user association problem in which each user would like to be associated with the BS that maximizes its throughput. However, one can see from (13) and (14) that the achievable user rates also depend on the existing user load on the BSs. Thus, a coupled relationship between the entities needs to be solved. To obtain a tractable solution, the BS-user association problem could be modeled as a one-to-many matching game. To this end, the goal of the first sub-problem P1 is to maximize the end-to-end sum rate of both BSs by optimizing users' BS selection with fixed values of Ψ and $\mathcal{H}$. The first sub-problem is formulated as follows

$$\begin{aligned} (\text{P1}): \quad & \max_{\hat{\mathcal{K}}} \quad \Phi_{GBS} + \Phi_{UAV} \\ & \text{s.t.} \quad (15), (16). \end{aligned} \tag{19}$$

Note that the objective in P1 could be achieved by developing a user association matrix where each user is allowed to be associated with the BS that offers a higher transmission rate. The weather attenuation condition can also affect user association and achievable user throughput, and the matching GT could provide an adaptive solution that responds to the prevailing weather.

In this game, we have two disjoint sets of players, the set of users $\mathcal{K}$ and the set of BSs $\mathcal{M}$. Note that each user $k \in \mathcal{K}$ could be associated with one BS $m \in \mathcal{M}$ at a time. To this end, the matching cell association problem is determined by the tuple $(\mathcal{K}, \mathcal{M}, \mathcal{Z}^m, \succ_{\mathcal{K}}, \succ_{\mathcal{M}})$, where $\succ_{\mathcal{K}} = \{\succ_k\}_{k\in\mathcal{K}}$ and $\succ_{\mathcal{M}} = \{\succ_m\}_{m\in\mathcal{M}}$ define the preference list of users' and BSs, respectively. Note that $\succ$ denotes the preference notation and $\mathcal{Z}^m$ is the quota vector of the BSs. One can note that in adverse weather, all users might want to switch to the UAV. In favorable weather, the opposite could happen. Hence, limiting the number of user associations with the BSs could be counterproductive. Thus, it is assumed that the quota vector $\mathcal{Z}^m$ can house up to K users for both BSs. In the matching GT, if a particular user is matched to a BS, it can be also interpreted as the BS being matched to that user [47]. The matching is mathematically defined as follows.

Definition 1. *A utility matching function $\mathcal{U}$ represents the BS–user association problem which can be expressed as a function from the set $\mathcal{K} \cup \mathcal{M}$ into the set $\mathcal{K} \cup \mathcal{M}$ such that*

- $|\mathcal{U}(k)| \leq 1$ *and* $\mathcal{U}(k) \in \mathcal{M} \cup \emptyset$;
- $|\mathcal{U}(m)| \leq \mathcal{Z}^m, \forall m \in \mathcal{M}$;
- $m \in \mathcal{U}(k)$ *if and only if* $\mathcal{U}(m) = k$.

where $\mathcal{U}(.)$ is the matching outcome and $|\mathcal{U}(.)|$ denotes its cardinality.

Definition 2. *A matching $\mathcal{U}$ with link $(k, m) \in \mathcal{U}$ is considered to be stable if there exists no matching $\mathcal{U}^k_{m,m'}$, such that the kth user favors BS m to $m^{'}$ (or vice versa), $\forall k \in \mathcal{K}$ or BS m prefers user $k^{'}$ to k, $\forall m \in \mathcal{M}$. In addition, a matching could be blocked by the BS (i.e., the user is not permitted to change BS) for a BS–user pair $(\mathcal{U}(m), m)$ if $\mathcal{U}(m) \neq k$ and $k \succ_m \mathcal{U}(m)$.*

Hence, an outcome of a stable matching is a bilateral assignment to all players. An iterative matching permits the kth user to iterate its matching if and only if it is beneficial in terms of the attained utility U_k. Specifically, the users build their preferences relation based on the achievable throughput using both BSs. For any kth user and the two BSs $m, m' \in \mathcal{M}$, $m \neq m'$, two possible matches exist, $\mathcal{U}$,$\mathcal{U}' \in \mathcal{K} \cup \mathcal{M}$, $m = \mathcal{U}(k)$, $m' = \mathcal{U}'(k)$. To this end, we have the following properties:

$$\begin{aligned} m \succ_k m' \Leftrightarrow \; & U_k(m) > U_k(m') \\ \Leftrightarrow \; & \mathcal{R}^m_k > \mathcal{R}^{m'}_k \end{aligned} \tag{20}$$

where $m \succ_k m'$ indicates that the user $k \in \mathcal{K}$ prefers BS m as opposed to BS m' due to a higher achievable throughput (utility) with BS m. In addition, for BS m and any two users $k, k' \in \mathcal{K}, k \neq k'$, two possible matches exist, $\mathcal{U}, \mathcal{U}' \in \mathcal{K} \cup \mathcal{M}, k = \mathcal{U}(m), k' = \mathcal{U}'(m)$, and we have the following properties:

$$\begin{aligned} k \succ_m k' \Leftrightarrow & \ U_m(k) > U_m(k') \\ \Leftrightarrow & \ \mathcal{R}_k^m > \mathcal{R}_{k'}^m \end{aligned} \tag{21}$$

One can note from (20) and (21) that the matching preferences of the players are related to their utilities, which are governed by the achievable data rates defined in (13) and (14).

Iterative Matching Game Procedure

Algorithm 1 outlines the proposed iterative matching procedure, which involves iterative matching until network-wide stability is attained. All users are initially assumed to be associated with the BS with the highest RSRP. Each user creates a list of preferred BSs and requests to be associated with their preferred BS. Both BSs also construct their preference lists depending on the total rate they offer to the associated users. Each BS also gives a ranking score to the users based on their preference list. Note that the user preference relations are interdependent, as they are influenced by the existing matching (i.e., the individual user data rate could change with a change in user load on the BS). This type of matching is categorized as matching with peer effects [48]. Users would only seek a change in serving BS if the other BS provided a better data rate. Additionally, the BS agent approves the request if the requesting user increases the BS's overall ranking; otherwise, it rejects it. Usually, a user would not request a change of BS which needs to be blocked, as under the proposed scheme, increasing the user's data rate also increases the BS rate and the ranking score. The blocking mechanism would only be activated if an abnormal request is received. The procedure is iteratively updated, and the algorithm returns a stable matching $\mathcal{U}^*$ when no user would like to change its association. It is worth emphasizing that an outcome of Algorithm 1 could vary if the weather condition changes i.e., change in ϑ.

Algorithm 1: Optimal User Association Using Iterative Matching Game

Initialize: User association based on RSRP in (10),
All users create a preference list $\succ k$ over both BSs
Both BSs create a preference list $\succ m$ over all users
Result: Convergence to a stable matching $\mathcal{U}^*$
while an iterative matching exists $\mathcal{U}_{m,m'}^k$ such that k prefers m'*to* m, $(k, m) \in \mathcal{U}$ **do**
  Each user k contacts their preferred BS m
  BSs rank the users in decreasing order
  if $rank(K_m + 1) > rank(K_m)$ **then**
    Discard the user from the preference list $\succ m$;
    Associate the applicant user to BS $m^{'}$;
    Discard BS m from preference list $\succ k$;
  else
    BS $m^{'}$ blocks the proposal of user k ;
  end
  Users $\forall k$ rebuild a fresh preference list $\succ k$ on current matching
  BSs $\forall m$ rebuild a fresh preference list $\succ m$ on current matching
end
Stable matching: $\mathcal{U}^*$ which gives $\hat{\mathcal{K}}, \bar{\Phi}_{UAV}, \bar{\Phi}_{GBS}$

Note that Algorithm 1 is guaranteed to converge to a final matching for the given weather attenuation from any initial user association. There are only two BSs; we can

determine a fixed number of user transfers in the network, and each user only intends to change BS if it improves its data rate. That is, with the specified parameters Ψ and $\mathcal{H}$, it is clear that in a network with a fixed number of users and BSs, user gain is always limited, meaning users could only conduct a finite number of transfers to maximize their gain. The number of transfers are mainly dictated by the weather attenuation coefficient ϑ. Hence, the while loop of Algorithm 1 is guaranteed to terminate after a certain number of steps when no user could improve their data rate. The convergence ensures the stability of the association, as no user would have a desire to deviate from their final BS–user association.

3.2. Resource Optimization Using Reinforcement Learning

Note that Algorithm 1 solves P1 to maximize the network sum throughput using the matching GT method and produces $\bar{\Phi}_{GBS}$ and $\bar{\Phi}_{UAV}$, the end-to-end network throughput of the GBS and the UAV, respectively. This is achieved by supplying a fixed combination of bandwidth partition factor Ψ, and the UAV altitude $\mathcal{H}$ as the optimization problem involving these parameters becomes intractable due to coupled relationships. However, it is crucial to determine the optimal values of both Ψ and $\mathcal{H}$, as both parameters could significantly impact not only the user association but also the individual user rates and total network throughput. We need to iteratively invoke Algorithm 1 to optimize the sum of $\bar{\Phi}_{GBS}$ and $\bar{\Phi}_{UAV}$. Since a nearly optimal solution necessitates a large number of iterations, we exploit RL to obtain a joint optimization of $\mathcal{H}$ and Ψ by periodically invoking Algorithm 1 to optimize the sum of $\bar{\Phi}_{GBS}$ and $\bar{\Phi}_{UAV}$. To this end, the optimization problem P2 is presented as

$$\begin{aligned} (\text{P2}): \quad & \max_{\Psi,\mathcal{H}} \quad \bar{\Phi}_{GBS} + \bar{\Phi}_{UAV} \\ & \text{s.t.} \quad (17), (18). \end{aligned} \tag{22}$$

In RL, an agent continuously interacts with the environment, taking various actions in response to new conditions (states) presented by the environment. The agent obtains a reward from the environment after completing an action. The reward can be positive if the action was desirable or negative (e.g., a penalty) if the action was unfavorable. One of the most popular RL methods is Q-learning [49] in which the agent learns the action–value function Q, which represents the expected reward against a state–action pair (s_t, a_t). It is considered that the UAV agent takes both actions (modifying the UAV altitude and bandwidth partition). This assumption simplifies the model because the UAV must act according to weather attenuation and the GBS and UAV need minimal communication. For instance, the UAV would share the bandwidth partition parameter while the GBS only needs to share its total end-to-end throughput values in return after each iteration. To this end, the state–action value function of the UAV agent could be iteratively updated as

$$Q(s_{t+1}, a_{t+1}) \leftarrow Q(s_t, a_t) + \alpha[r_{t+1} + \nu \max_{a} Q(s'_t, a'_t)], \tag{23}$$

where α and ν represent the learning rate and discount factor, respectively. In this paper, UAV functions as an agent for the Q-learning model, which is composed of four components: states, actions, rewards, and the Q-value. The objective of Q-learning is to develop a policy that maximizes observed rewards over the duration of the agent's interactions. Note that we employ Q-learning because we could formulate the problem with a finite state and action space and because it is an efficient algorithm for this type of problem. If the state space was large, we could have used other RL methods such as deep Q-network (DQN), which approximates Q-values for state–action pairs using a deep neural network (DNN). Figure 3 depicts the working principle of RL in the proposed framework.

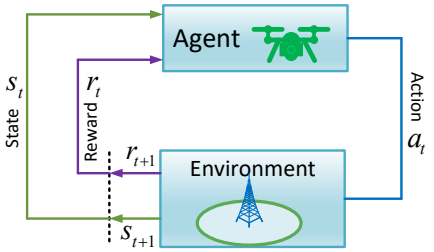

Figure 3. The working principle of reinforcement learning.

3.2.1. State Representation

The UAV agent employs a state model comprised of $\varrho = (\mathcal{H}_{UAV}, \Psi_{UAV})$, where $\mathcal{H}_{UAV}$ is the altitude of UAV and Ψ_{UAV} denotes the bandwidth partition between the UAV and GBS. The state for a UAV deployment can be denoted as $\mathcal{H}_{UAV} : \{\mathcal{H}_{min}, ..., \mathcal{H}_{max}\}$, $\Psi_{UAV} : \{\Psi_{min}, ..., \Psi_{max}\}$.

3.2.2. Action Space

The agent carries out an action $a_t \in$ A at each step, which comprises a combination of altitude $\mathcal{H}$ (increase or decrease) and bandwidth partition Ψ (increase or decrease) based on the decision policy $\mathcal{V}$, which is determined in the Q-table, $Q(s_t, a_t)$.

3.2.3. State Transition Model

A transition from s_t to s_{t+1} having reward r_t at action a_t is characterized by the conditional transition probability $p(s_{t+1}, r_t | s_t, a_t)$. By exploiting Q-learning, we aim to maximize the long-term reward $\mathcal{J}_t$ for the given weather attenuation condition, which can be stated as

$$\mathcal{J}_t = \mathrm{E}\left[\sum_{n=0}^{\infty} \nu^n r_{t+n}\right], \tag{24}$$

where ν is the discount factor and the reward is calculated based on the objective function in P2 as explained below.

3.2.4. Rewards

Without loss of generality, the reward function is formulated by the total network throughput $\bar{\Phi}_s = \bar{\Phi}_{GBS} + \bar{\Phi}_{UAV}$ for the given weather attenuation. If the action that the UAV carries out at current time t can improve $\bar{\Phi}_s$, then the UAV receives a positive reward. The UAV agent receives a negative reward otherwise. Hence, the reward function can be stated as [50]

$$r_t = \begin{cases} 1, & \text{if } \bar{\Phi}_{s,\text{new}} > \bar{\Phi}_{s,\text{old}}, \\ -0.1, & \text{if } \bar{\Phi}_{s,\text{new}} = \bar{\Phi}_{s,\text{old}}, \\ -1, & \text{if } \bar{\Phi}_{s,\text{new}} < \bar{\Phi}_{s,\text{old}}. \end{cases} \tag{25}$$

Algorithm 2 outlines the complete RL approach for solving P2. The plot in Figure 4 depicts the algorithm's convergence for the use-case of $V = 0.8$ km. It is worth noting that the algorithm converges in approximately 1800 episodes, each of which has 250 steps.

Remark 1. *It is also worth noting that the system is trained for random user distributions with uniform statistics, while the convergence for a more predictable user distribution is expected to be substantially faster. After training, the model can quickly determine optimal values $\mathcal{H}_{opt}$ and Ψ_{opt} for any user distribution. (The non-uniform and clustered user distribution will be considered in future work.)*

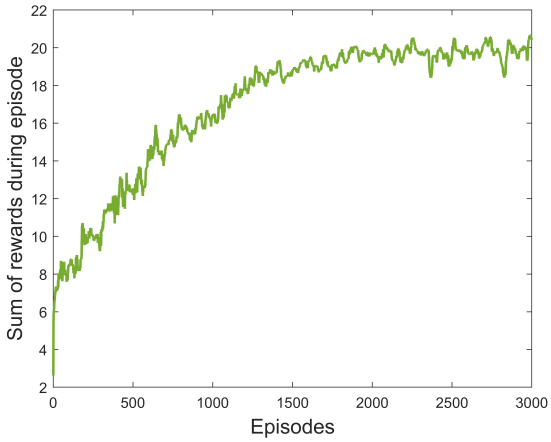

Figure 4. Convergence of the Q-Learning algorithm; based on our experiments, it converges within around 1800 episodes.

Algorithm 2: Q-Learning Algorithm for UAV Deployment and Resource Partition Optimization

Input : Altitude lower $\mathcal{H}_{min}$ and upper $\mathcal{H}_{edge}$ bounds,
Bandwidth allocation factor
Lower Ψ_{min} and upper Ψ_{max} bounds,
Coverage radius R, episodes $\mathcal{N}$, steps $\mathcal{T}$

Output: Q-table containing $Q(s,a)$ values defining optimal policy π^*,
Optimal UAV altitude $\mathcal{H}_{opt}$,
Optimal bandwidth allocation factor Ψ_{opt}

initialize;
Altitude values $\mathcal{H}_{min}$ to $\mathcal{H}_{edge}$ with step size δ_h
Bandwidth factor Ψ_{min} to Ψ_{max} with step size δ_Ψ
Learning rate $\alpha \leftarrow 0.1$
Discount factor $\nu \leftarrow 0.95$
Exploration factor $\epsilon \leftarrow 1$
Init. Q-table for all state-action pairs $Q(s,a) \leftarrow 0$
for *episode* $\leftarrow 0 : \mathcal{N}$ **do**
  Reset state $s_0 \leftarrow (\mathcal{H}_{min}, \Psi_{min})$
  for $t \leftarrow 0 : \mathcal{T}$ **do**
    $a \leftarrow \begin{cases} \arg\max_a Q(s_t,a_t), & \text{prob. } 1-\epsilon, \\ random_a\, Q(s_t,a_t), & \text{prob. } \epsilon, \end{cases}$
    Compute reward r_{t+1} for action a using P2
    Update Q-table for s_t, a_t, r_{t+1} combination:
    $Q(s_{t+1},a_{t+1}) \leftarrow Q(s_t,a_t) + \alpha[r_{t+1} + \nu \max_a Q(s'_t,a'_t)]$
  end
  Update value of epsilon $\epsilon \leftarrow \epsilon - \dfrac{\epsilon}{\mathcal{N}-1}$
end

3.3. Additional Performance Metric

The main goal of the proposed scheme is to maximize the end-to-end system throughput and allow users to associate with the preferable BS. However, we could also consider other important metrics to evaluate and compare the performance of the systems. To this end, we employ Jain's fairness index, which is an important measure of fairness, and it is defined as [51,52]

$$\mathcal{Q} = \frac{(\sum_{k=1}^{K} \mathcal{R}_k)^2}{K \sum_{k=1}^{K} \mathcal{R}_k^2}, \tag{26}$$

where $\mathcal{R}_k$ represents the data rate of the kth user, irrespective of its associated BS. In comparison to other measures, Jain's index has a fairness criterion that considers all system users, not only the users that are allocated minimal resources. Note that $\mathcal{Q}$ lies in the range $\left[\frac{1}{K}, 1\right]$ where $\mathcal{Q}$ =1 corresponds to the fairest allocation; i.e., every user receives the same data rate.

3.4. Complexity and Convergence Analysis

The computational complexity of the Q-learning algorithm scales linearly with the number of states and the number of actions [53]. The complexity of the proposed Algorithm 2 is the same as Q-learning, which is $\mathcal{O}(\mathcal{S}\mathsf{A})$. Since our action-space consists of only four actions, the complexity could be reduced to only $\mathcal{O}(\mathcal{S})$. Note that we can obtain a tradeoff between the accuracy and model complexity when the discretization of state-space is appropriately chosen. The complexity of the matching GT-based Algorithm 1 depends on the number of user association transfers T. Therefore, the complexity of the proposed framework is $\mathcal{O}(\mathcal{S}\mathsf{T})$. Moreover, studies have proved that both Q-learning [53] and the matching game [47] are guaranteed to converge if sufficient iterations are provided.

4. Numerical Results and Discussion

In this section, we present some simulation results for our proposed system as an application of user offloading during the adverse weather conditions as plotted in Figure 1. Unless otherwise stated, the values of the system parameters used for the numerical simulations are listed in Table 1. The AWGN noise power is assumed to be $N_{\mathrm{p}} = -90$ dBm [10,54]. In addition, a moderate turbulence condition with $C_n^2 = 1.7 \times 10^{-14}\mathrm{m}^{-2/3}$ [55] is considered. The minimum threshold capacity C_{th} of the FSO link corresponds to the weather-attenuation coefficient $\vartheta = 10$ dB/km.

Note that CUDE is a suboptimal CURE scheme with lower complexity. That is, the UAV deployment (i.e., altitude) under the CUDE scheme is based on (9), while the bandwidth partitioning factor Ψ is optimized to maximize the total network throughput, and it follows the same matching GT procedure as the CURE scheme. The benchmark CARE model uses a bias parameter for cell range expansion (CRE) [56] to encourage user association with the UAV. The CRE technique virtually increases the user's received power by adding a bias value to balance the user load and improve the system's performance. Otherwise, almost all users would like to be associated with the GBS under the maximum RSRP policy since the transmit power of UAV is practically lower than that of GBS. It is worth noting that the CARE scheme does not consider the backhaul condition, and it employs an equal bandwidth (i.e., $\frac{W}{K}$) allocation policy to all users.

Firstly, we plot the individual BS throughput and user association probability as a function of weather attenuation coefficient ϑ for the proposed CURE scheme in Figure 5. Note that user association probability could be defined as the ratio of the number of users connected to a specific BS to the total number of users. One can see that both individual BS throughput and user association probability are an increasing and decreasing function of the weather attenuation coefficient ϑ for the UAV and GBS, respectively. That is, as ϑ increases, the capacity of the FSO backhaul diminishes, causing an increasing number of users to migrate from the GBS to the UAV, which illustrates the importance of UAV deployment during an infrequent foggy weather situation. In addition, Figure 6 shows the optimal UAV altitude $\mathcal{H}_{opt}$ and bandwidth allocation factor Ψ_{opt} against an increasing weather attenuation coefficient ϑ. As the weather deteriorates, the UAV is assigned more bandwidth resources so that it could offload more users and increase total system throughput; also, as the FSO backhaul becomes less reliable, the UAV's altitude is increased to cover the entire cell. As the optimal value of both parameters varies, it emphasizes the need for optimizing these parameters with regard to a particular weather attenuation condition.

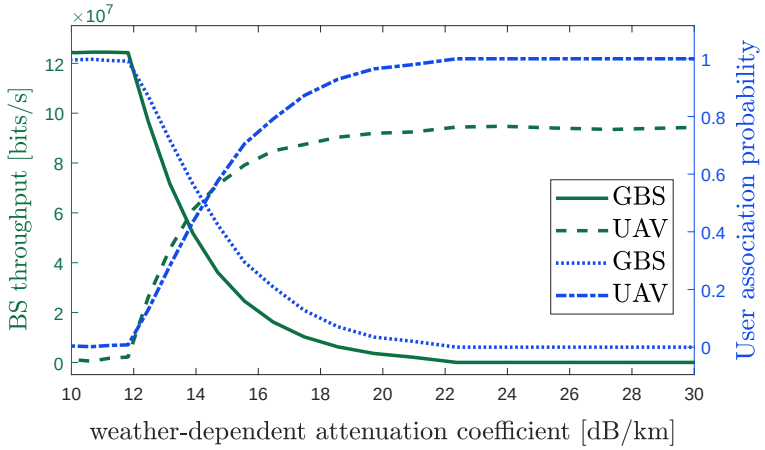

Figure 5. Individual BS throughput and user association probability as a function of increasing weather-attenuation coefficient for CURE model.

Table 1. Simulation parameters.

FSO Link [6]		
Parameter	**Symbol**	**Value**
FSO wavelength	λ_o	1550 nm
Receiver diameter	d	5 cm
Beam divergence	ϕ	3.5 mrad
Refraction structure index	C_n^2	1.7×10^{-14} m$^{-2/3}$
Responsivity	ρ	0.5V^{-1}
Noise variance	σ_o^2	10^{-14}A^2
Transmit power	ζ_o	20 dBm
Bandwidth	W_o	1 GHz
Link distance	$L_{\mathcal{SD}}$	1000 m
RF Link (Downlink) [10,11]		
Parameter	**Symbol**	**Value**
Carrier frequency	f_c	2 GHz
Bandwidth	W	20 MHz
Number of users	K	300
GBS transmit power	$\zeta_{\mathrm{T}}^{\mathrm{s}}$	30 dBm
UAV transmit power	$\zeta_{\mathrm{T}}^{\mathrm{a}}$	20 dBm
Pathloss exponent	η	2
Additional path loss LoS, NLoS	Γ_1, Γ_2	3 dB, 23 dB
Environment parameter	ω_1, ω_2	12.08, 0.11
AWGN noise power	N_{p}	-90 dBm

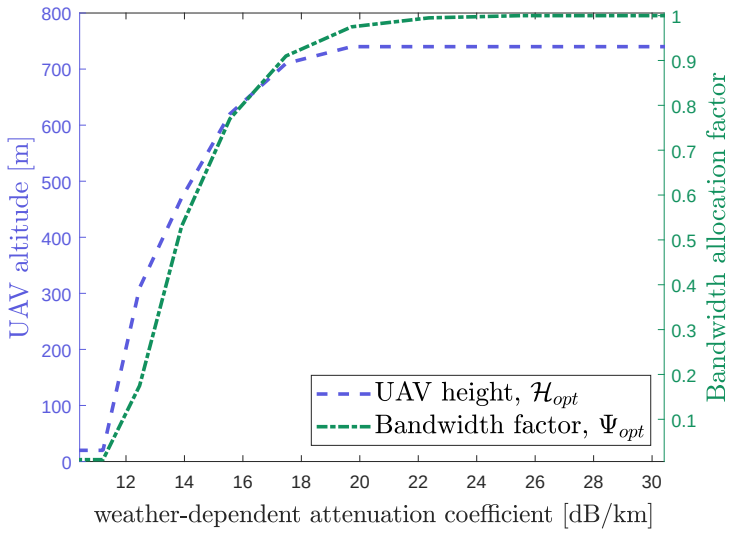

Figure 6. Optimal UAV altitude and bandwidth partition between two BSs as a function of increasing weather-attenuation coefficient ϑ for the proposed CURE model.

We illustrate the user association between the GBS and the UAV for the proposed CURE scheme under three low-visibility conditions for the conventional case in Figure 7 wherein the transmit power of GBS is higher than the UAV i.e., $\zeta_{\mathrm{T}}^{\mathrm{s}} > \zeta_{\mathrm{T}}^{\mathrm{a}}$. The users associated with the GBS and the UAV are represented by the blue and orange dots (100 trials), respectively. Under a low visibility situation in Figure 7a,b, the UAV tends to cover the majority of users in the middle of the coverage region, whereas the GBS covers some users closer to the origin and at the edges. This is particularly interesting because due to the relatively high weather attenuation at visibility $V = 0.8$ km, the GBS backhaul cannot support many users which are offloaded to the UAV. More interestingly, since the UAV's access link is weaker than that of the GBS (due to its lower transmit power) despite a better UAV–user LoS channel, it hovers at an intermediate altitude to cover users in the middle of the cell. In fact, this inhibits the use of exclusive inner and outer ring coverage (e.g., [10]) for the GBS and UAV, respectively, when the GBS backhaul is not reliable. However, as the visibility increases further in Figure 7c to 0.9 km, the GBS backhaul is relatively more reliable, but it is not entirely capable of supporting all access traffic. Thus, the UAV is pushed to cover users in the center rather than at the edges due to the UAV's limited transmit power, and it also hovers at a low altitude (e.g., 184 m).

On the other hand, when the transmit power of both the BSs is comparable in Figure 8 (equal in this case, $\zeta_{\mathrm{T}}^{\mathrm{s}} = \zeta_{\mathrm{T}}^{\mathrm{a}}$), the GBS's coverage shrinks to a small region close to the origin. Note that this situation is not practical because UAVs have limited power and their transmit power is usually not comparable to that of a GBS; rather, these results are plotted to show how the system behaves when both BSs have comparable transmit powers. One can note that in all three visibility scenarios presented in Figure 8, the UAV covers most of the cell (outer region) because it has a better channel and same transmit power level that offers an advantage; therefore, more users would like to be associated with the UAV. However, the UAV would tend to fly at a higher altitude to cover the entire cell, which allows the users closer to the origin to prefer GBS compared to the UAV. As visibility improves, the altitude of the UAV increases because the GBS with a more reliable backhaul can support more users closer to the origin, and the UAV serves the majority of the users away from the origin to maximize total network throughput.

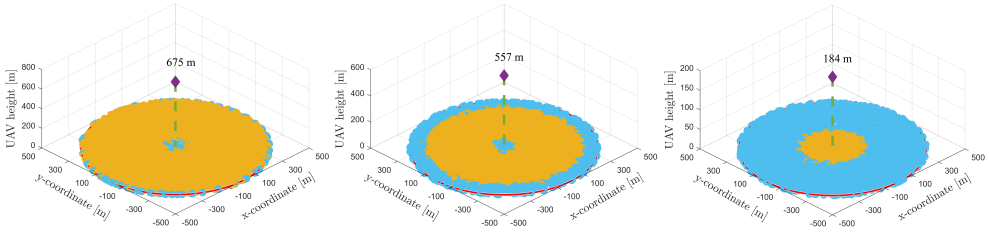

(**a**) $V = 0.7$ km (**b**) $V = 0.8$ km (**c**) $V = 0.9$ km

Figure 7. Three–dimensional (3D) coverage map and UAV altitude for three low-visibility regimes when $\zeta_{\mathrm{T}}^{\mathrm{s}} > \zeta_{\mathrm{T}}^{\mathrm{a}}$; the blue and orange dots represent users associated with the GBS and UAV, respectively.

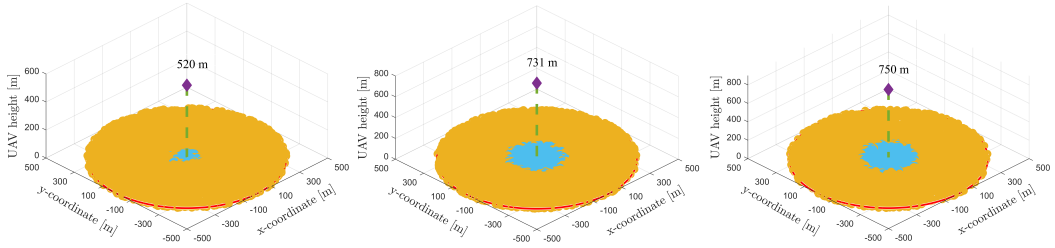

(**a**) $V = 0.7$ km (**b**) $V = 0.8$ km (**c**) $V = 0.9$ km

Figure 8. Three–dimensional (3D) coverage map and UAV altitude for three low visibility regimes when $\zeta_{\mathrm{T}}^{\mathrm{s}} = \zeta_{\mathrm{T}}^{\mathrm{a}}$; the blue and orange dots represent users associated with the GBS and UAV, respectively.

The results in Figure 9 show the superior system throughput performance of the proposed CURE scheme over the conventional user association methods. It is evident that the proposed suboptimal CUDE model exhibits closer performance to the CURE scheme compared to the other benchmark cases. However, the performance limitation is caused by the traditional UAV placement method (edge user-based UAV deployment) despite the implementation of a backhaul-aware user association policy. One can note that the CARE scheme's performance, in both cases of 5 dB and 10 dB of added power for CRE, deteriorates as the weather attenuation increases. This is because the user association disregards the FSO link reliability and only cares about access link conditions. As expected, the performance of GBSO increasingly deteriorates as the weather attenuation increases, because the FSO backhaul becomes more unreliable as ϑ increases. The proposed CURE scheme achieves the best total system throughput performance and offers users the flexibility to choose their preferred BS to enhance their user experience. However, it is worth assessing the impact of this objective on the fairness of the users. To do this, we employ the widely used Jain's fairness index $\mathcal{Q}$, as outlined in (26). The results in Figure 10 clearly illustrate that the proposed CURE scheme offers good fairness results to the users, while the fixed altitude case of the proposed model (i.e., CUDE, which is also backhaul-aware but with a fixed UAV altitude) leads in terms of fairness performance. It is worth noting here that the Jain's fairness index evaluates the disparity of the data rates within an individual scheme. That is, if a scheme has very low system throughput (e.g., GBSO in Figure 9), it can still be very fair if all the users have comparable data rates. The GBSO scheme is a classic illustration of this situation, as shown in Figure 10.

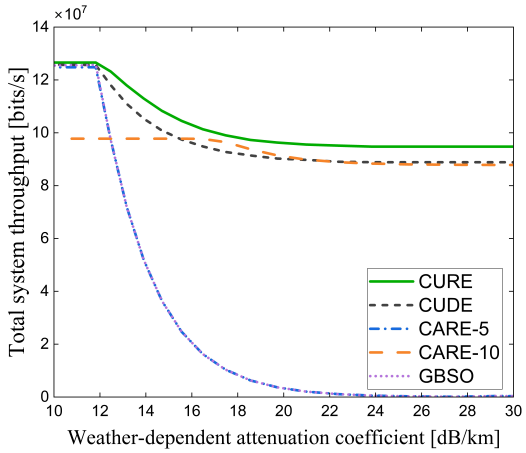

Figure 9. Total system throughput of all the models versus the weather-dependent attenuation coefficient ϑ of the FSO link.

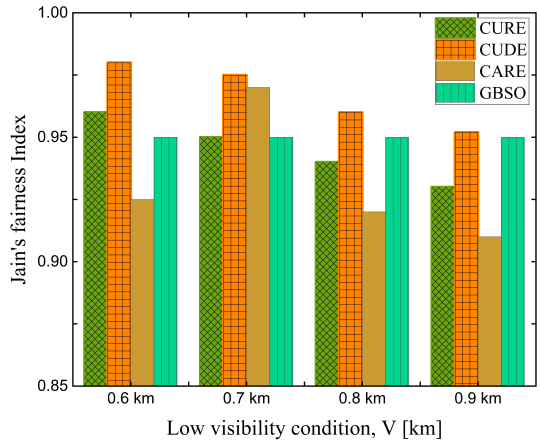

Figure 10. Fairness performance of all the schemes under four low-visibility conditions.

We now evaluate how our system would perform in a realistic channel model that uses climate data from the cities of Edinburgh and London. Figure 11 plots the histogram of hourly visibility for Edinburgh and London as reported by the United Kingdom Meteorological Office for January 2019 to June 2020, totaling H_{tot} = 13,106 h (Edinburgh), H_{tot} = 13,128 h (London). As can be seen, the probability of fog events (visibility $<$ 1 km) which can severely deteriorate the FSO link's performance is very small. Because FSO links function well most of the time, fixed hybrid FSO/RF links with permanent or backup RF links are not necessarily the most cost-effective and practical solution all the time [6]. To this end, it encourages researchers to come up with short-term solutions such as the one proposed here. These approaches might play a significant role in B5G networks where UAVs can offload traffic from the BS during rare low-visibility situations.

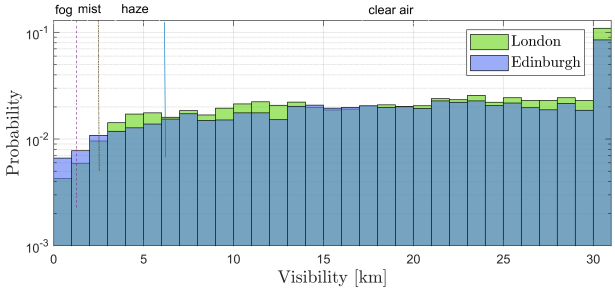

Figure 11. Hourly visibility histogram for Edinburgh and London from January 2019 to June 2020.

We use fog events to simulate the total system throughput using the hourly visibility data, with low visibility hours H_{fog} of 87 and 56 for Edinburgh and London, respectively. Figure 12 demonstrates that the proposed CURE scheme outperforms the other systems, including the GBSO, CUDE, and CARE scheme during the fog events in both cities. When visibility is near 1 km, the CUDE and CARE schemes rarely perform comparably to the proposed CURE scheme. On the other hand, the CURE scheme performs well throughout the fog events in both London and Edinburgh, even when the counterpart models perform poorly. For example, during fog hour 26 and 30 in Edinburgh and London, respectively, the GBSO's throughput is almost zero, while the CURE scheme still offers better throughput compared to the CUDE and CARE scheme in both Edinburgh and London.

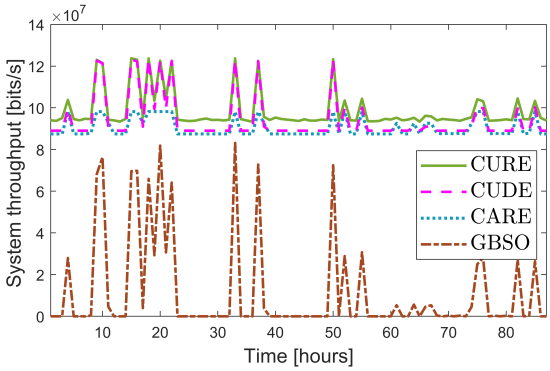

(**a**) Edinburgh

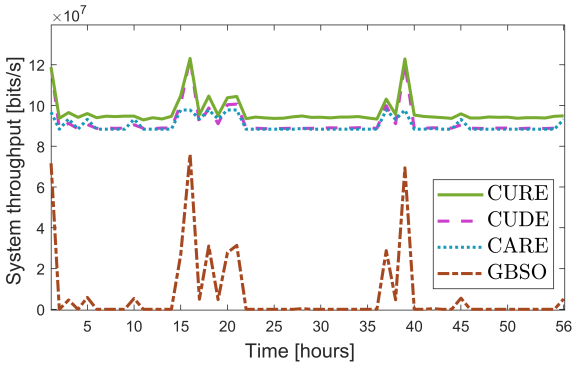

(**b**) London

Figure 12. The end-to-end system throughput of the proposed and benchmark schemes versus the fog hours in Edinburgh and London from January 2019 to June 2020.

5. Conclusions

A novel hybrid FSO/RF system based on the matching game theory and RL is proposed in this study with the use of UAV-assisted user offloading. Originally, only the GBS is serving the coverage area, and no UAV is assumed to be involved. However, when the infrequent adverse weather strikes to impair the FSO link's availability, the GBS can be augmented by a UAV. It helps to establish a dual-hop RF link to maintain its throughput to the MBS by using a portion of the RF spectrum from the GBS node. The problem is solved using a layered framework, where the user association is performed using a matching-game while the UAV's altitude optimization and bandwidth resource sharing with the GBS are optimized using RL. Numerical simulations demonstrate that the proposed approach can considerably increase the system's total throughput under the adverse weather conditions when compared to the FSO-only and other benchmark schemes. A realistic channel based on Edinburgh and London weather records was used to evaluate the proposed system's performance; the proposed system showed a significant increase in throughput which can increase the network availability over the other schemes. With the expected exponential growth of FSO nodes in B5G networks, the findings of this study motivate the

development of temporary and practical UAV-assisted FSO backhaul solutions. These condition-aware hybrid FSO/RF systems will optimize the network performance during rare weather situations, which considerably hamper the FSO link's capacity.

Author Contributions: Conceptualization, M.N., S.H. and M.S.; Methodology, M.N., S.H. and M.S.; Validation, S.H. and M.S.; Investigation, M.N.; Writing—original draft, M.N.; Writing—review and editing, M.N., S.H., J.T. and M.S.; Visualization, M.N.; Supervision, J.T. and M.S.; Project administration, M.N. and S.H.; Funding acquisition, M.S. All authors have read and agreed to the published version of the manuscript.

Funding: The work of Majid Safari was supported by the Engineering and Physical Sciences Research Council (EPSRC) through the Terabit Bidirectional Multi-User Optical Wireless System (TOWS) for 6G LiFi under Program EP/S016570/1.

Institutional Review Board Statement: Not applicable.

Informed Consent Statement: Not applicable.

Data Availability Statement: Not applicable.

Acknowledgments: The authors are grateful to the Meteorological Office of the United Kingdom for supplying measured hourly temperature and visibility data for January 2019 to June 2020 from the Edinburgh Gogarbank and the London Heathrow weather stations.

Conflicts of Interest: The authors declare that there is no conflict of interest.

Abbreviations

The following abbreviations are used in this manuscript:

AWGN	additive white Gaussian noise
B5G	beyond fifth-generation
BS	base station
CRE	cell range expansion
FSO	free-space optical
GBS	ground base station
GBSO	GBS only
GT	game theory
IM/DD	intensity modulation direct detection
MBS	macro base station
ML	machine learning
QoS	quality of service
RF	radio frequency
RL	reinforcement learning
RSRP	reference signal received power
UAVs	unmanned aerial vehicles

References

1. Jiang, W.; Han, B.; Habibi, M.A.; Schotten, H.D. The Road Towards 6G: A Comprehensive Survey. *IEEE Open J. Commun. Soc.* **2021**, *2*, 334–366. [CrossRef]
2. Ullah, Z.; Al-Turjman, F.; Mostarda, L. Cognition in UAV-Aided 5G and Beyond Communications: A Survey. *IEEE Trans. Cogn. Commun. Netw.* **2020**, *6*, 872–891. [CrossRef]
3. Dang, S.; Amin, O.; Shihada, B.; Alouini, M.S. What should 6G be? *Nat. Electron.* **2020**, *3*, 20–29. [CrossRef]
4. Bekkali, A.; Fujita, H.; Hattori, M. New Generation Free-Space Optical Communication Systems With Advanced Optical Beam Stabilizer. *J. Light. Technol.* **2022**, *40*, 1509–1518. [CrossRef]
5. Agheli, P.; Emadi, M.J.; Beyranvand, H. Cognitive RF-FSO Fronthaul Assignment in Cell-Free and User-Centric mMIMO Networks. *IEEE Trans. Mob. Comput.* **2021**. [CrossRef]
6. Huang, S.; Shah-Mansouri, V.; Safari, M. Game-Theoretic Spectrum Trading in RF Relay-Assisted Free-Space Optical Communications. *IEEE Trans. Wirel. Commun.* **2019**, *18*, 4803–4815. [CrossRef]
7. Yahia, O.B.; Erdogan, E.; Kurt, G.K.; Altunbas, I.; Yanikomeroglu, H. A Weather-Dependent Hybrid RF/FSO Satellite Communication for Improved Power Efficiency. *IEEE Wirel. Commun. Lett.* **2022**, *11*, 573–577. [CrossRef]

8. Hassan, M.Z.; Hossain, M.J.; Cheng, J.; Leung, V.C.M. Hybrid RF/FSO Backhaul Networks With Statistical-QoS-Aware Buffer-Aided Relaying. *IEEE Trans. Wirel. Commun.* **2020**, *19*, 1464–1483. [CrossRef]
9. Zhou, M.; Chen, H.; Shu, L.; Liu, Y. UAV-Assisted Sleep Scheduling Algorithm for Energy-Efficient Data Collection in Agricultural Internet of Things. *IEEE Internet Things J.* **2022**, *9*, 11043–11056. [CrossRef]
10. Ali, M.A.; Jamalipour, A. UAV-Aided Cellular Operation by User Offloading. *IEEE Internet Things J.* **2021**, *8*, 9855–9864. [CrossRef]
11. Hu, Z.; Zheng, Z.; Song, L.; Wang, T.; Li, X. UAV offloading: Spectrum trading contract design for UAV-assisted cellular networks. *IEEE Trans. Wirel. Commun.* **2018**, *17*, 6093–6107. [CrossRef]
12. Lyu, J.; Zeng, Y.; Zhang, R. UAV-Aided Offloading for Cellular Hotspot. *IEEE Trans. Wirel. Commun.* **2018**, *17*, 3988–4001. [CrossRef]
13. Yan, H.; Bao, W.; Zhu, X.; Wang, J.; Liu, L. Data Offloading Enabled by Heterogeneous UAVs for IoT Applications under Uncertain Environments. *IEEE Internet Things J.* **2022**. [CrossRef]
14. Kouhdaragh, V.; Verde, F.; Gelli, G.; Abouei, J. On the application of machine learning to the design of UAV-based 5G radio access networks. *Electronics* **2020**, *9*, 689. [CrossRef]
15. Fan, B.; Jiang, L.; Chen, Y.; Zhang, Y.; Wu, Y. UAV Assisted Traffic Offloading in Air Ground Integrated Networks With Mixed User Traffic. *IEEE Trans. Intell. Transp. Syst.* **2022**, *23*, 12601–12611. [CrossRef]
16. Mukherjee, A.; Misra, S.; Chandra, V.S.P.; Obaidat, M.S. Resource-Optimized Multiarmed Bandit-Based Offload Path Selection in Edge UAV Swarms. *IEEE Internet Things J.* **2019**, *6*, 4889–4896. [CrossRef]
17. Gao, A.; Wang, Q.; Liang, W.; Ding, Z. Game Combined Multi-Agent Reinforcement Learning Approach for UAV Assisted Offloading. *IEEE Trans. Veh. Technol.* **2021**, *70*, 12888–12901. [CrossRef]
18. Asheralieva, A.; Niyato, D. Hierarchical Game-Theoretic and Reinforcement Learning Framework for Computational Offloading in UAV-Enabled Mobile Edge Computing Networks With Multiple Service Providers. *IEEE Internet Things J.* **2019**, *6*, 8753–8769. [CrossRef]
19. Li, L.; Ren, H.; Cheng, Q.; Xue, K.; Chen, W.; Debbah, M.; Han, Z. Millimeter-Wave Networking in the Sky: A Machine Learning and Mean Field Game Approach for Joint Beamforming and Beam-Steering. *IEEE Trans. Wirel. Commun.* **2020**, *19*, 6393–6408. [CrossRef]
20. Zhang, S.; Ansari, N. 3D Drone Base Station Placement and Resource Allocation With FSO-Based Backhaul in Hotspots. *IEEE Trans. Veh. Technol.* **2020**, *69*, 3322–3329. [CrossRef]
21. Lee, J.H.; Park, K.H.; Ko, Y.C.; Alouini, M.S. Spectral-Efficient Network Design for High-Altitude Platform Station Networks With Mixed RF/FSO System. *IEEE Trans. Wirel. Commun.* **2022**, *21*, 7072–7087. [CrossRef]
22. Wang, J.Y.; Ma, Y.; Lu, R.R.; Wang, J.B.; Lin, M.; Cheng, J. Hovering UAV-Based FSO Communications: Channel Modelling, Performance Analysis, and Parameter Optimization. *IEEE J. Sel. Areas Commun.* **2021**, *39*, 2946–2959. [CrossRef]
23. Ajam, H.; Najafi, M.; Jamali, V.; Schober, R. Ergodic Sum Rate Analysis of UAV-Based Relay Networks With Mixed RF-FSO Channels. *IEEE Open J. Commun. Soc.* **2020**, *1*, 164–178. [CrossRef]
24. Che, Y.L.; Long, W.; Luo, S.; Wu, K.; Zhang, R. Energy-Efficient UAV Multicasting With Simultaneous FSO Backhaul and Power Transfer. *IEEE Wirel. Commun. Lett.* **2021**, *10*, 1537–1541. [CrossRef]
25. Zhang, S.; Ansari, N. Latency Aware 3D Placement and User Association in Drone-Assisted Heterogeneous Networks With FSO-Based Backhaul. *IEEE Trans. Veh. Technol.* **2021**, *70*, 11991–12000. [CrossRef]
26. Kouzayha, N.; Elsawy, H.; Dahrouj, H.; Alshaikh, K.; Al-Naffouri, T.Y.; Alouini, M.S. Analysis of Large Scale Aerial Terrestrial Networks with mmWave Backhauling. *IEEE Trans. Wirel. Commun.* **2021**, *20*, 8362–8380. [CrossRef]
27. Zeng, Y.; Lyu, J.; Zhang, R. Cellular-Connected UAV: Potential, Challenges, and Promising Technologies. *IEEE Wirel. Commun.* **2019**, *26*, 120–127. [CrossRef]
28. Jamali, V.; Michalopoulos, D.S.; Uysal, M.; Schober, R. Link allocation for multiuser systems with hybrid RF/FSO backhaul: Delay-limited and delay-tolerant designs. *IEEE Trans. Wirel. Commun.* **2016**, *15*, 3281–3295. [CrossRef]
29. Kim, I.I.; Koontz, J.; Hakakha, H.; Adhikari, P.; Stieger, R.; Moursund, C.; Barclay, M.; Stanford, A.; Ruigrok, R.; Schuster, J.J.; et al. Measurement of scintillation and link margin for the TerraLink laser communication system. *Proc. SPIE* **1998**, *3232*, 100–118. [CrossRef]
30. Nistazakis, H.E.; Tsiftsis, T.A.; Tombras, G.S. Performance analysis of free-space optical communication systems over atmospheric turbulence channels. *IET Commun.* **2009**, *3*, 1402–1409. [CrossRef]
31. Al-Habash, A.; Andrews, L.C.; Phillips, R.L. Mathematical model for the irradiance probability density function of a laser beam propagating through turbulent media. *Opt. Eng.* **2001**, *40*, 1554–1562. [CrossRef]
32. He, B.; Schober, R. Bit-interleaved coded modulation for hybrid RF/FSO systems. *IEEE Trans. Commun.* **2009**, *57*, 3753–3763. [CrossRef]
33. Lapidoth, A.; Moser, S.M.; Wigger, M.A. On the capacity of free-space optical intensity channels. *IEEE Trans. Inf. Theory* **2009**, *55*, 4449–4461. [CrossRef]
34. Farid, A.A.; Hranilovic, S. Outage Capacity Optimization for Free-Space Optical Links With Pointing Errors. *J. Light. Tech.* **2007**, *25*, 1702–1710. [CrossRef]
35. Izadpanah, H.; ElBatt, T.; Kukshya, V.; Dolezal, F.; Ryu, B. High-availability free space optical and RF hybrid wireless networks. *IEEE Wirel. Commun.* **2003**, *10*, 45–53. [CrossRef]

36. Nafees, M.; Thompson, J.; Safari, M. Multi-Tier Variable Height UAV Networks: User Coverage and Throughput Optimization. *IEEE Access* **2021**, *9*, 119684–119699. [CrossRef]
37. Mozaffari, M.; Saad, W.; Bennis, M.; Debbah, M. Mobile Unmanned Aerial Vehicles (UAVs) for Energy-Efficient Internet of Things Communications. *IEEE Trans. Wirel. Commun.* **2017**, *16*, 7574–7589. [CrossRef]
38. Khuwaja, A.A.; Zheng, G.; Chen, Y.; Feng, W. Optimum Deployment of Multiple UAVs for Coverage Area Maximization in the Presence of Co-Channel Interference. *IEEE Access* **2019**, *7*, 85203–85212. [CrossRef]
39. Namvar, N.; Homaifar, A.; Karimoddini, A.; Maham, B. Heterogeneous UAV Cells: An Effective Resource Allocation Scheme for Maximum Coverage Performance. *IEEE Access* **2019**, *7*, 164708–164719. [CrossRef]
40. Azari, M.M.; Rosas, F.; Chen, K.; Pollin, S. Ultra Reliable UAV Communication Using Altitude and Cooperation Diversity. *IEEE Trans. Commun.* **2018**, *66*, 330–344. [CrossRef]
41. Al-Hourani, A.; Kandeepan, S.; Lardner, S. Optimal LAP Altitude for Maximum Coverage. *IEEE Wirel. Commun. Lett.* **2014**, *3*, 569–572. [CrossRef]
42. Qian, C.; Zhang, W.; Zhou, W. Performance Evaluation of Reference Signal Received Power Strength Based Idle Users' Cell Selection in 3GPP LTE. In Proceedings of the 2013 IEEE 77th Vehicular Technology Conference (VTC Spring), Dresden, Germany, 2–5 June 2013; pp. 1–5. [CrossRef]
43. Ghimire, J.; Rosenberg, C. Revisiting Scheduling in Heterogeneous Networks When the Backhaul Is Limited. *IEEE J. Sel. Areas Commun.* **2015**, *33*, 2039–2051. [CrossRef]
44. Nadeem, F.; Kvicera, V.; Awan, M.S.; Leitgeb, E.; Muhammad, S.S.; Kandus, G. Weather effects on hybrid FSO/RF communication link. *IEEE J. Sel. Areas Commun.* **2009**, *27*, 1687–1697. [CrossRef]
45. Mkiramweni, M.E.; Yang, C.; Li, J.; Zhang, W. A Survey of Game Theory in Unmanned Aerial Vehicles Communications. *IEEE Commun. Surv. Tutorials* **2019**, *21*, 3386–3416. [CrossRef]
46. LeAnh, T.; Tran, N.H.; Saad, W.; Le, L.B.; Niyato, D.; Ho, T.M.; Hong, C.S. Matching Theory for Distributed User Association and Resource Allocation in Cognitive Femtocell Networks. *IEEE Trans. Veh. Technol.* **2017**, *66*, 8413–8428. [CrossRef]
47. Sekander, S.; Tabassum, H.; Hossain, E. Decoupled Uplink-Downlink User Association in Multi-Tier Full-Duplex Cellular Networks: A Two-Sided Matching Game. *IEEE Trans. Mobile Comput.* **2017**, *16*, 2778–2791. . [CrossRef]
48. Gu, Y.; Saad, W.; Bennis, M.; Debbah, M.; Han, Z. Matching theory for future wireless networks: Fundamentals and applications. *IEEE Commun. Mag.* **2015**, *53*, 52–59. [CrossRef]
49. Jang, B.; Kim, M.; Harerimana, G.; Kim, J.W. Q-Learning Algorithms: A Comprehensive Classification and Applications. *IEEE Access* **2019**, *7*, 133653–133667. [CrossRef]
50. Liu, X.; Liu, Y.; Chen, Y. Reinforcement Learning in Multiple-UAV Networks: Deployment and Movement Design. *IEEE Trans. Veh. Technol.* **2019**, *68*, 8036–8049. [CrossRef]
51. Jain, R.K.; Chiu, D.M.W.; Hawe, W.R. *A Quantitative Measure of Fairness and Discrimination*; Eastern Research Laboratory, Digital Equipment Corporation: Hudson, MA, USA, 1984; Volume 21.
52. Sediq, A.B.; Gohary, R.H.; Schoenen, R.; Yanikomeroglu, H. Optimal Tradeoff Between Sum-Rate Efficiency and Jain's Fairness Index in Resource Allocation. *IEEE Trans. Wirel. Commun.* **2013**, *12*, 3496–3509. [CrossRef]
53. Valente Klaine, P.; Jaber, M.; Souza, R.D.; Imran, M.A. Backhaul Aware User-Specific Cell Association Using Q-Learning. *IEEE Trans. Wirel. Commun.* **2019**, *18*, 3528–3541. [CrossRef]
54. Zeng, F.; Hu, Z.; Xiao, Z.; Jiang, H.; Zhou, S.; Liu, W.; Liu, D. Resource Allocation and Trajectory Optimization for QoE Provisioning in Energy-Efficient UAV-Enabled Wireless Networks. *IEEE Trans. Veh. Technol.* **2020**, *69*, 7634–7647. [CrossRef]
55. Shakir, W.M.R. Performance evaluation of a selection combining scheme for the hybrid FSO/RF system. *IEEE Photon. J.* **2017**, *10*, 7901110. [CrossRef]
56. Muhammad, F.; Abbas, Z.H.; Li, F.Y. Cell Association With Load Balancing in Nonuniform Heterogeneous Cellular Networks: Coverage Probability and Rate Analysis. *IEEE Trans. Veh. Technol.* **2017**, *66*, 5241–5255. [CrossRef]